

# Crystal plasticity investigation of friction effect on texture evolution of Al single crystal during ECAP

G. Y. Deng · C. Lu · A. K. Tieu · L. H. Su ·  
N. N. Huynh · X. H. Liu

Received: 11 February 2010/Accepted: 28 May 2010/Published online: 10 June 2010  
© Springer Science+Business Media, LLC 2010

**Abstract** A crystal plasticity finite element model has been developed to study the effect of friction between the die wall and the billet on texture evolution during equal channel angular pressing of an aluminum single crystal. Four cases with different coefficients of friction  $\mu = 0, 0.05, 0.1$ , and  $0.15$  have been simulated. It has been found that the friction of  $\mu = 0.05$  and  $0.1$  can capture the major texture features shown in the experimental results, and  $\mu = 0.05$  predicts a slightly better texture than  $\mu = 0.1$ . The frictional condition significantly affects texture evolution in the region between  $1/2$  and  $3/4$  of the billet thickness from the top surface. It can be attributed to the effect of friction on the corner gap and the distribution of stresses in the die corner.

## Introduction

Equal channel angular pressing (ECAP), one of the promising severe plastic deformation (SPD) technique due to its capability of manufacturing bulk specimens with ultrafine-grained (UFG) structure in a wide range of bulk metals and alloys, has been extensively studied over the last two decades [1, 2]. In ECAP, the billets are inserted

and extruded through a die that contains two equal cross-sectional channels meeting at a predetermined angle ( $\Phi$ ), and the process can be easily repeated to impose a large plastic strain. It has been known that the microstructure and texture of materials processed by ECAP depend mainly on the accumulative strain route and pass number and strongly relate to the material properties, such as strain hardening exponent and strain rate sensitivity [1–6]. Friction between the billet and the channels also significantly affects the texture evolution during the ECAP pressing. Segal [7], followed by Mathieu et al. [8] and Hockauf et al. [9], has used sliding parts to experimentally control friction in ECAP-batch processing. Friction was also controlled in the continuous ECAP processes [10, 11].

The finite element method (FEM) is a very important and reliable computer-aided analysis tool for simulations of ECAP. A number of FEM analyses concerning the effect of friction in ECAP have been conducted [12–17]. Prangnell et al. [12] have carried out the first finite element analysis of ECAP. They reported a corner gap formed in the outer die corner, resulting in nonuniform strain distribution in the billet. It has been found that strain and inhomogeneous deformation increases with friction. Yang and Lee [13] found that friction condition does not affect the strain distribution. Li et al. [14] reported that friction has little effect on the shape of the plastic deformation zone (PDZ) when the material fills the die. However, it had some effects on the local variation of strain rates at the inner and outer corner regions. Specifically, an increase of friction leads to a higher plastic strain rate in the inner corner and variation of the strain rates near the outer corner region. Wei et al. [15] revealed that the strain distribution is relatively more uniform with friction than that without friction. They attributed the reason to the back pressure induced by friction and concluded that friction is not the

G. Y. Deng · X. H. Liu  
State Key Lab of Rolling and Automation, Northeastern  
University, Shenyang 110004, China

G. Y. Deng · C. Lu (✉) · A. K. Tieu · L. H. Su · N. N. Huynh  
School of Mechanical, Materials and Mechatronic Engineering,  
University of Wollongong, Wollongong, NSW 2522, Australia  
e-mail: chengl@uow.edu.au

L. H. Su  
School of Materials and Metallurgy, Northeastern University,  
Shenyang 110004, China

source of nonuniform strain distribution. Balasundar and Raghu [17] compared the effects of the Coulomb and shear friction models in the simulation of ECAP. All the above-mentioned studies adopted the classic constitutive law for plastic deformation, which is unable to predict texture evolution, and focused their discussions on the effects of friction on the distributions of strain or/and strain rate. Texture models, such as full constraints (FC) Taylor-type model and visco-plastic self-consistent (VPSC) model, have been applied to predict texture evolution during ECAP with the deformation histories determined by FEM [5, 18, 19]. However, numerical investigation of the effect of friction on texture in ECAP has not been seen in the published literatures.

Full constraints Taylor-type model and VPSC model were applied to model the texture evolution of ECAP [20, 21]. The FC Taylor-type model assumes that the local strain rate equals to the macroscopic strain rate, while the VPSC model allows the strain rate of each grain being different not only from the macroscopic strain rate but also from those of neighboring grains. However, these studies decoupled the deformation history simulation and texture modeling, and gave unsatisfactory prediction. In this study, a crystal plasticity FEM (CPFEM) model, which incorporates crystal plasticity constitutive equations into a finite element framework, has been developed to understand the effect of friction between the die wall and the billet on texture evolution of aluminum single crystal with a well-defined initial orientation during ECAP. The constitutive law in CPFEM is based on the fact that plastic deformation occurs by crystallographic slips on the slip systems and the rotations of the crystal lattices. With the initial distribution of the crystallographic orientation, CPFEM can simulate the change of the orientation for each node and simultaneously calculate hardening and deformation response based on the applied boundary conditions. CPFEM models have been recognized as the best models for the simulation of plastic deformation of crystalline materials and for the prediction of deformation textures [22]. Li et al. [23] have shown that the CPFEM model exhibited better texture predictions than the VPSC model. The current CPFEM performs very well in the texture modeling of single crystal. It is limited in the texture modeling of polycrystalline materials due to grain to grain interaction. The strain gradient CPFEM under development aims to solve this problem. Using the developed CPFEM model, the effect of friction on texture evolution in ECAP will be analyzed in details in this paper.

## Finite element analysis

The crystal plasticity constitutive relations used here follow the line described by Asaro [24]. The details are given

in [25]. The crystal plasticity constitutive equations are implemented into the implicit finite element code ABAQUS/Standard using user material subroutine (UMAT). The major functions of UMAT are to provide the consistent tangent modulus (Jacobian matrix) as required for an iterative Newton–Raphson solution in ABAQUS, and to update stress and state variables including crystallographic orientation. We modified the UMAT framework initially developed by Huang [26] and incorporate Bassani and Wu model [27] into the hardening model.

The actual deformation history measured from scribed marker grids showed that the materials on the central plane of the ECAPed billet were subjected to the plane strain deformation [28]. Therefore, it is reasonable to assume a plane strain condition in the present simulation to reduce the computing time. In order to validate the developed CPFEM model, the ECAP die geometry used in the experiments of Ref. [29] is adopted in the present simulation. In the experiment as proposed in [29], the four longer faces of the sample were prepared to obtain a mirror-like finish by grinding on abrasive paper and electro-polishing and then coated in a MoS<sub>2</sub> lubricant prior to processing by ECAP. The single crystal was pressed partially through a split die fabricated from tool steel in a single pass, and the pressing was terminated when the crystal was essentially at the mid-point of the die. The ECAP die was then opened, and the sample carefully removed. A JSM-5600 scanning electron microscope equipped with an OIM capability was used to measure the crystallographic orientations. For OIM, the image area was set at  $150 \times 150 \mu\text{m}^2$  and individual measurements were taken periodically at incremental steps of  $1.5 \mu\text{m}$ . In the simulation, the angle ( $\Phi$ ) between two channels is  $90^\circ$ , and the angle of the die outer corner ( $\Psi$ ) is given by  $30^\circ$ . A small smooth fillet radius ( $r = 0.3 \text{ mm}$ ) is created in the die inner corner to avoid distortion of the mesh. The width of the channels is 4 mm. The billet has an initial rectangular shape of  $23.2 \times 4 \text{ mm}^2$ . The experimental and simulated results in Ref. [5] indicated that the unstable deformation occurred in the region with the distance less than a billet thickness from the leading end of the billet, beyond which texture exhibited stable results. The billet length in the present simulation is 5.8 times the billet thickness. It is long enough to reach the steady-state deformation condition. The billet is meshed by 6596 plane strain 4-node elements with reduced integration (element id: CPE4R). The total node number is 6369. Coulomb friction model with a limit of maximum shear stress has been used in the simulation. There are two popular friction models in metal forming: Coulomb friction and shear friction model. The former is suitable for low friction conditions (lubricated cold processes), while the latter can be used for high friction conditions (hot deformation). The

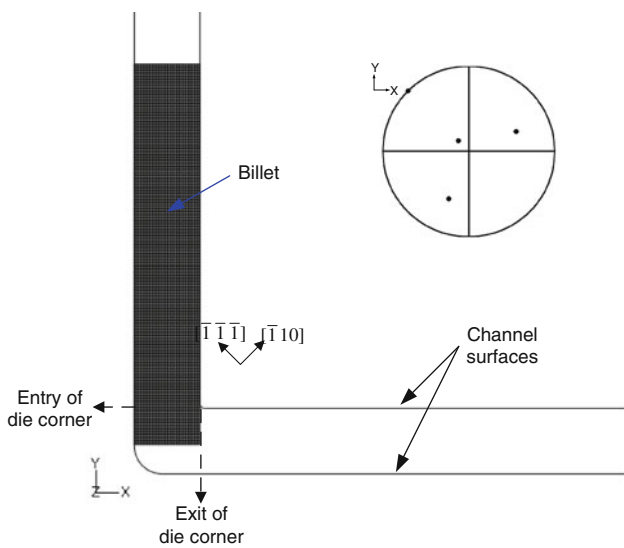


**Fig. 1** The configuration of the ECAP die and billet in the simulation and initial pole figure of the material

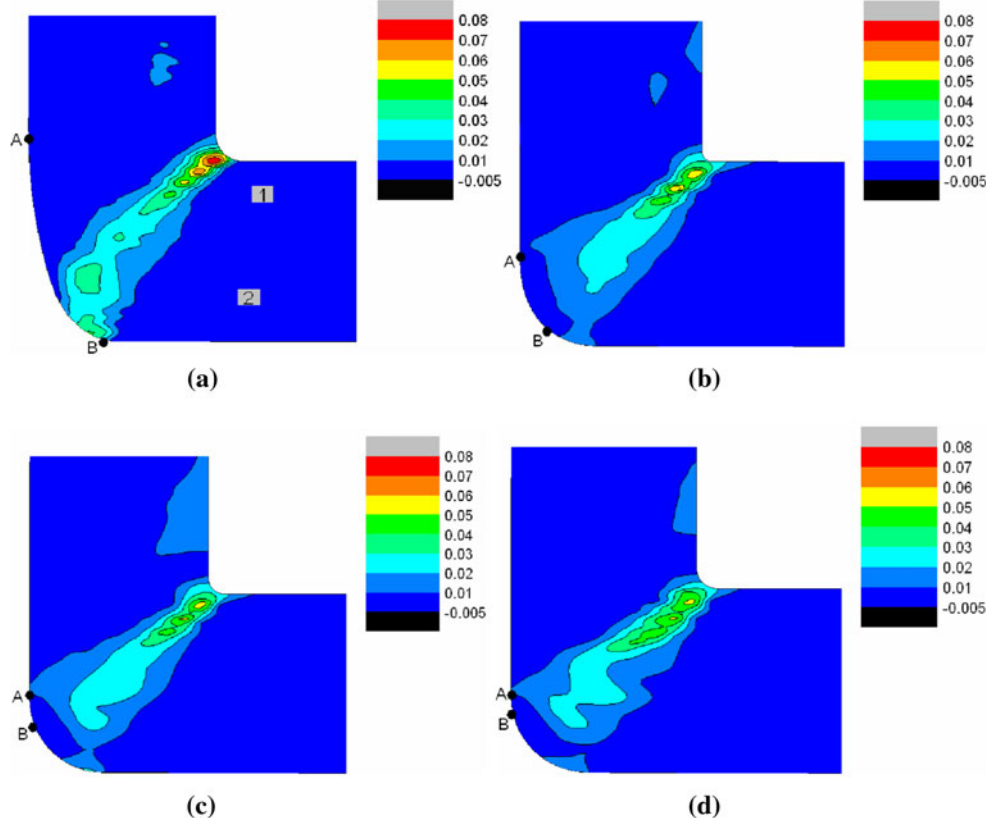
experiments in Ref. [29] were conducted at the room temperature and under MoS<sub>2</sub> lubrication conditions. Therefore, Coulomb friction model is chosen in the simulation. In Coulomb friction model, the frictional stress is assumed to be the coefficient of friction multiplied by the normal pressure. Four different coefficients of friction

( $\mu = 0, 0.05, 0.1$  and  $0.15$ ) have been used in the simulation to investigate the effect of friction on texture evolution. All simulations are carried out with a constant ram speed of  $0.056$  mm/s along the  $-Y$  direction and does not stop until the tail of the billet reaches the entry of the die corner. The simulated material is the aluminum single crystal with an identical initial orientation to the experiments of Ref. [29], namely, the  $\langle\bar{1}\bar{1}\bar{1}\rangle$  slip plane parallel to the ideal shear plane of the die, and the  $\langle\bar{1}10\rangle$  slip direction parallel to the direction of shear. Note that the coordinate system in Ref. [29] is left-handed, while our system is right-handed. A  $\{111\}$  pole figure of the initial orientation is shown in Fig. 1.

## Results and discussions

Figure 2 shows the distributions of equivalent strain rate ( $\dot{\epsilon}$ ) in the billets for different coefficients of friction at the time step where the top surface of the billet is  $4.2$  mm away from the entry of the die corner and the steady-state deformation has been reached. It can be seen that the deformation already occurs in a small area within the entry channel for the frictionless case (Fig. 2a). When friction is applied to the interface between the die wall and the billet (Fig. 2b–d), the deformation is induced in the vicinity of

**Fig. 2** Distribution of equivalent strain rate ( $s^{-1}$ ) in the billet. **a**  $\mu = 0$ ; **b**  $\mu = 0.05$ ; **c**  $\mu = 0.1$ ; and **d**  $\mu = 0.15$



the right-side interface in the entry channel and extends from the right side to the left side. It is clear that the plastic deformation zone (PDZ) in the die corner, represented by  $\dot{\varepsilon}$ , spreads about the intersection plane of the channels for all simulations and the effect of friction on the  $\dot{\varepsilon}$  distributions in the PDZ is obvious. Similar to the prediction of [5, 14], the equivalent strain rate significantly changes from the inner corner to the outer corner, and it has higher values in the inner corner than the central area and outer corner. Without friction, the PDZ is relatively narrow. For the cases with friction, the PDZ can be divided into two parts based on the pattern of  $\dot{\varepsilon}$ . The upper part of the PDZ has a fan-like shape. It covers the major portion of the PDZ. The lower part of the PDZ includes two small deformation regions near the billet surface, between which a rigid-rotation region exists. It has been found that a large corner gap exists for the frictionless case, while the corner gap almost disappears when the coefficient of friction is increased to 0.05. The billet material has filled in the whole die corner for cases with  $\mu = 0.1$  and 0.15, which is consistent with results reported by Li et al. [5]. However, a careful inspection indicates that there is a non-contact area between points A and B in the outer corner of the die. The non-contact area is not subjected to constraint force from the die wall. This will intensify the inhomogeneous deformation in the billet.

In order to validate the developed simulation model, the simulated {111} pole figures for four different coefficients of friction have been compared in Fig. 3 with the measured results [29] for two positions labeled 1 and 2 in Fig. 2a. The simulation model uses the same initial orientation as the experiments, as shown in Fig. 1. It should be noted that there are much less points in the simulated pole figures than the measured ones because the dimension of the elements is much larger than the resolution used in the experiments. For position 1 (upper panel of Fig. 3), the experimental observation shows that the structure remains a single

crystal and the crystallographic orientation has been rotated from the initial orientation. Fukuda et al. [29] interpreted that the rotation angle is 60° around the Z axis (Y axis in their paper) in the counter-clockwise sense. It can be seen from Fig. 3 that all simulation results are in good agreement with the measured one for position 1. This indicates that the developed model in this study can predict accurate texture and the texture at position 1 is not sensitive to friction. The measured pole figure at position 2 reveals a rotated orientation and an initial orientation. The simulation for the frictionless case only predicts the rotated orientation and the rotation angle is larger than the experimental value. The simulations with  $\mu = 0.05$  and 0.1 have predicted both initial orientation and rotated orientation. Compared with the experimental result (lower panel of Fig. 3a),  $\mu = 0.05$  exhibits a slightly better pole figure than  $\mu = 0.1$ . When the coefficient is increased to 0.15, except for the initial orientation, an unexpected orientation appears in the pole figure (lower panel in Fig. 3e). Comparisons in Fig. 3 indicate that a coefficient of friction between 0.05 and 0.1 can provide a good texture prediction.

In order to quantitatively analyze the rotation of the crystallographic orientation during ECAP, the misorientation of each node, which is calculated relative to the original orientation, is partitioned into three components which represent the rotation angles around the X, Y, and Z axes, respectively. The partition method proposed by Wert et al. [30] is adopted in this article. Contour maps of crystallographic orientation rotation angles around the X, Y, and Z axes for  $\mu = 0.1$  are shown in Fig. 4a–c, respectively. The positive value indicates the counter-clockwise (CCW) rotation and the negative value indicates the clockwise (CW) rotation. It can be seen from Fig. 4 that the crystallographic orientation rotates in three-dimension. The rotation angle around the Z axis is much larger than the other rotation directions. This is consistent with the

**Fig. 3** Comparisons of the {111} pole figures between simulations and experiment [29] (upper panel: position 1; lower panel: position 2). **a** Experiment; **b**  $\mu = 0$ ; **c**  $\mu = 0.05$ ; **d**  $\mu = 0.1$ ; **e**  $\mu = 0.15$

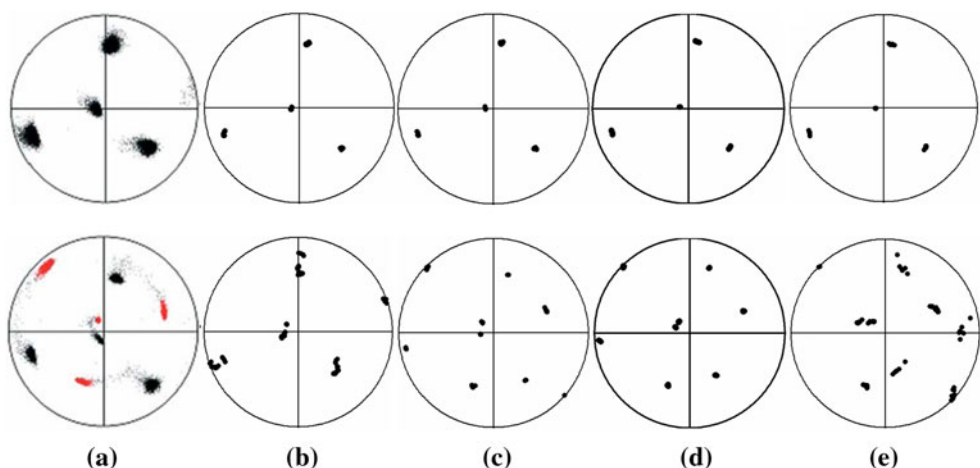
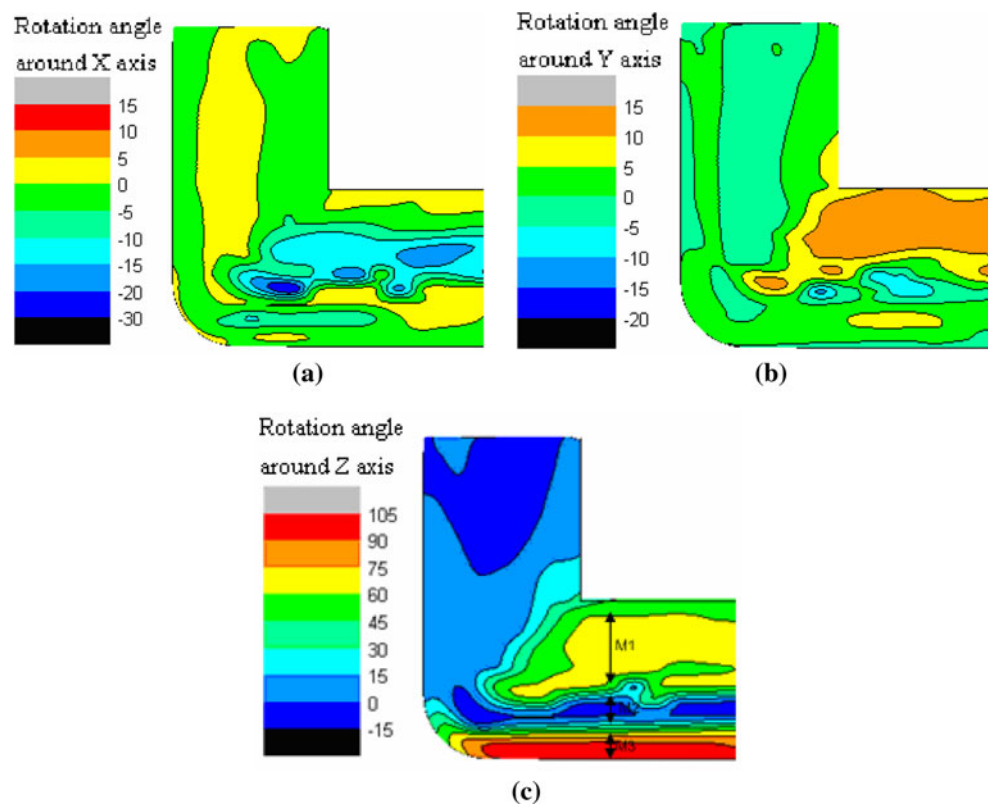


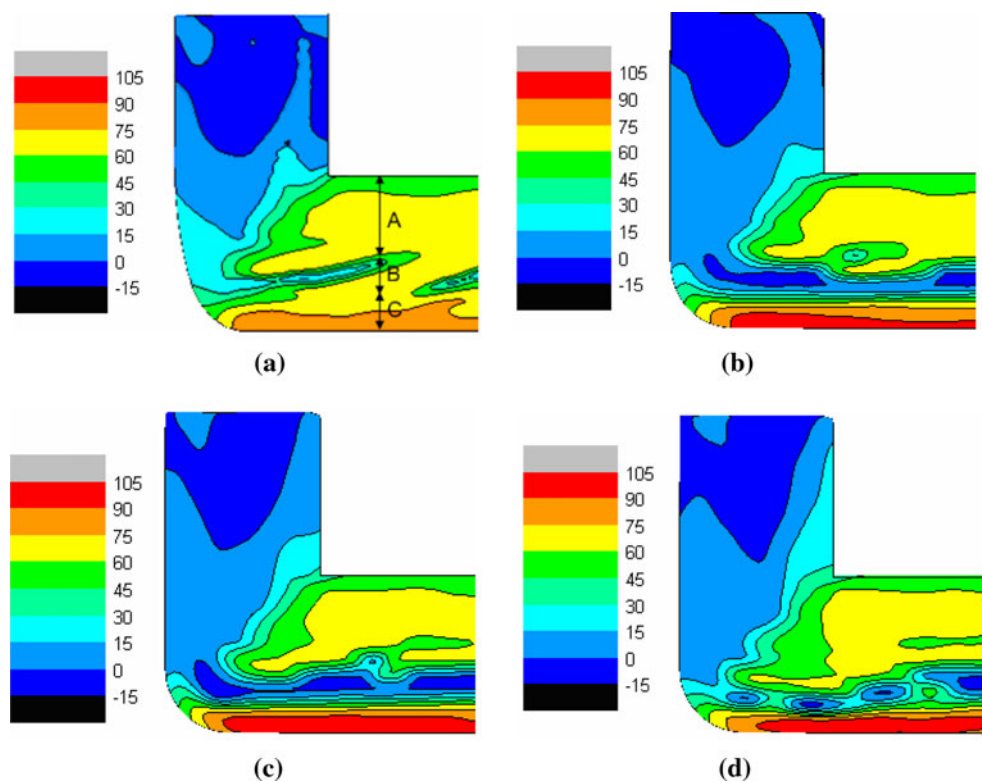
**Fig. 4** Distributions of rotation angles (degree) in the billet ( $\mu = 0.1$ ). **a** Contour map of rotation angle around X axis; **b** contour map of rotation angle around Y axis; **c** contour map of rotation angle around Z axis



experimental observations of single crystal and polycrystalline materials that the orientation mainly rotates around the transverse direction (TD) in ECAP [29, 31], which coincides with the Z axis shown in Fig. 1. In Fig. 4a, rotation angles around the X axis in the middle part of the billet are larger than those in the top and bottom parts. The distribution of the rotation angle around the Y axis is different from that around the X axis. The large-rotation area in Fig. 4b locates in the top part of the billet, while in the bottom part, the rotation angle around the Y axis is very small. According to the distribution of the rotation angle around the Z axis as shown in Fig. 4c, the deformed billet can be divided into three regions: top half part with about 60° Z axis rotation, the region between 1/2 and 3/4 of the billet thickness from the top surface with about 0° Z axis rotation and the rest region with about 90° Z axis rotation. Liu et al. [32] conducted cold rolling of cubic-oriented aluminum single crystal. They found that the crystal rotated mainly around TD and the crystal was subdivided macroscopically and symmetrically into four parts, designated matrix bands, along the thickness by the TD rotation. The rotation angle significantly varies in the regions between matrix bands, defined as transient bands. Figure 4c depicts that there are three matrix bands through the thickness of the ECAP-ed billet. They are defined as M1, M2, and M3, respectively. The TD rotation angles in three matrix bands are about 60°, 0° and 90°, respectively.

Similar to  $\mu = 0.1$ , the simulations for other coefficients of friction also show that the lattice mainly rotates around the Z axis. Therefore, we only compare the rotation angles around the Z axis for four coefficients of friction in Fig. 5. For the convenience of analysis, the billet is divided into three regions, marked A, B and C, along the billet thickness as shown in Fig. 5a. The regions A, B and C roughly correspond to three matrix bands M1, M2 and M3 for the case of  $\mu = 0.1$ , respectively. All simulations predict a similar 60° Z axis rotation in the upper part of the deformed billet, namely Region A. It seems that friction does not affect texture in the main portion of Region A. A careful inspection shows that the Z axis rotation angle in the vicinity of the top surface of the deformed billet increases slightly with the coefficient of friction. This is due to the direct frictional effect on the top surface. Comparison in Fig. 5 shows that friction significantly affects the texture evolution in the lower part of the deformed billet, namely Regions B and C. The frictionless condition does not generate the initial orientation in Region B. A striation with a Z axis rotation angle of about 25° is inserted in the region with 60° Z axis rotation. In addition, the Z axis rotation angle in Region C for the frictionless case is smaller than other cases. It has been found in Fig. 5b and c that cases of  $\mu = 0.05$  and 0.1 exhibit similar results. Three matrix bands for both cases are parallel to the X axis. This indicates that the texture is heterogeneous

**Fig. 5** Rotation angles (degree) around the Z axis for different coefficients of friction. **a**  $\mu = 0$ ; **b**  $\mu = 0.05$ ; **c**  $\mu = 0.1$ ; and **d**  $\mu = 0.15$



along the billet thickness, but it is homogeneous along the X axis. When a higher friction ( $\mu = 0.15$ ) is applied, as shown in Fig. 5d, Region C near the bottom surface has a similar rotation angle to  $\mu = 0.05$  and 0.1. However, the case of  $\mu = 0.15$  has a different texture pattern in Region B. The texture is no longer homogeneous along the X axis in Region B of Fig. 5d. This region is partitioned into several small matrix bands. Based on above analysis, it can be found that the major texture difference for various coefficients of friction locates in Region B. The frictionless condition does not generate initial orientation in Region B. Continuous matrix bands with initial orientation are formed in the cases of  $\mu = 0.05$  and 0.1, while a higher friction ( $\mu = 0.15$ ) forms separate small matrix bands in Region B. It is clear from Fig. 5 that the texture evolution in Region B inherits from the PDZ. Therefore, it can be concluded that the frictional condition affects the texture in Region B through the PDZ. The inhomogeneous matrix bands in Region B also results in more rotation around the axes X and Y in the pole figure, as shown in Fig. 3e. As the friction is increased, the backpressure in the exit channel is increased, resulting in a smaller corner gap. The difference in the corner gap significantly affects the distribution of stresses in the lower part of the PDZ, but it affects little in the upper part of the PDZ. Therefore, the texture in Region B is dependent on the frictional condition, while the texture in Region A does not change. The texture in Region C is mainly determined by the rigid rotation, which is strongly

relative to the die geometry. Therefore, friction has a slight influence on the texture in Region C.

## Conclusions

- (1) A crystal plasticity FEM has been developed to investigate the effect of friction between the die wall and the billet on texture evolution during ECAP of an aluminum single crystal. The developed model has been validated by comparison with the experimental observation.
- (2) Four cases with different coefficients of friction of  $\mu = 0, 0.05, 0.1$ , and  $0.15$  have been simulated. It has been found that the coefficients of friction of  $\mu = 0.05$  and 0.1 can capture the major texture features shown in the experimental results and  $\mu = 0.05$  predicts a slightly better texture than  $\mu = 0.1$ .
- (3) The frictional condition significantly affects texture evolution in the region (Region B) between  $1/2$  and  $3/4$  of the billet thickness from the top surface. Cases of  $\mu = 0.05$  and 0.1 predict a matrix band with an initial orientation in this region and the matrix band is parallel to the X axis. However, this matrix band does not appear in the simulation with  $\mu = 0$ . When the coefficient of friction is high ( $\mu = 0.15$ ), Region B consists of separate small matrix bands. Friction

affects the texture in Region B through the PDZ. Different friction condition changes the shape of the corner gap and in turn influences the distribution of stresses in the lower part of the PDZ. As a result, the texture in Region B is different for different friction conditions.

**Acknowledgments** The authors acknowledge the financial support from an Australia Research Council Discovery Grant (DP0773329). G. Y. Deng and L. H. Su would like to thank the financial support from China Scholarship Council.

## References

1. Valiev RZ, Langdon TG (2006) *Prog Mater Sci* 51:881
2. Zhu YT, Langdon TG (2004) *JOM* 56:58
3. Semiatin SL, Delo DP, Shell EB (2000) *Acta Mater* 48:1841
4. Moon BS, Kim HS, Hong SI (2002) *Scr Mater* 46:131
5. Li S, Beyerlein IJ, Necker CT, Alexander DJ, Bourke M (2004) *Acta Mater* 52:4859
6. Su CW, Lu L, Lai MO (2007) *Mater Sci Technol* 23:727
7. Segal VM (2004) *Mater Sci Eng A* 386:269
8. Mathieu JP, Suwas S, Eberhardt A, Toth LS, Moll P (2006) *J Mater Process Technol* 173:29
9. Hockauf M, Meyer LW, Kruger L (2008) *Mater Sci Forum* 584–586:685
10. Lee JC, Seok HK, Suh JY (2002) *Acta Mater* 50:4005
11. Raab GJ, Valiev RZ, Lowe TC, Zhu YT (2004) *Mater Sci Eng A* 382:30
12. Prangnell PB, Harris C, Roberts SM (1997) *Scr Mater* 37:983
13. Yang YL, Lee S (2003) *J Mater Process Technol* 140:583
14. Li S, Bourke MAM, Beyerlein II, Alexander DJ, Clausen B (2004) *Mater Sci Eng A* 382:217
15. Wei W, Nagasekhar AV, Chen G, Tick-Hon Y, Wei KX (2006) *Scr Mater* 54:1865
16. Xu S, Zhao G, Ma X, Ren G (2007) *J Mater Process Technol* 184:209
17. Balasundar I, Raghu T (2010) *Mater Des* 31:449
18. Suh JY, Han JH, Oh KH, Lee JC (2003) *Scr Mater* 49:185
19. Li S, Beyerlein IJ, Alexander DJ, Vogel SC (2005) *Scr Mater* 52:1099
20. Ferrasse S, Segal VM, Kalidindi SR, Alford F (2004) *Mater Sci Eng A* 368:28
21. Li S, Beyerlein IJ, Bourke MAM (2005) *Mater Sci Eng A* 394:66
22. Wenk HR, Van Houtte P (2004) *Rep Prog Phys* 67:1367
23. Li S, Kalidindi SR, Beyerlein IJ (2005) *Mater Sci Eng A* 410–411:207
24. Asaro RJ (1983) *J Appl Mech Trans ASME* 50:921
25. Si LY, Lu C, Huynh NN, Tieu AK, Liu XH (2008) *J Mater Process Technol* 201:79
26. Huang YG (1991) *Mech Report* 178. Division of Engineering and Applied Sciences, Harvard University, Cambridge, Massachusetts
27. Bassani JL, Wu TY (1991) *Proc R Soc Lond A* 435:21
28. Ghoshal A, Bate P, Prangnell PB (2002) *Acta Mater* 50:2121
29. Fukuda Y, Ohishi K, Furukawa M, Horita Z, Langdon TG (2004) *Acta Mater* 52:1387
30. Wert JA, Liu Q, Hansen N (1997) *Acta Mater* 45:2565
31. Beyerlein IJ, Toth LS (2009) *Prog Mater Sci* 54:427
32. Liu Q, Maurice C, Driver J, Hansen N (1998) *Metall Mater Trans A Phys Metall Mater Sci* 29:2333